ZnO Nanocrystals

DOI: 10.1002/anie.201106201

# Synthesis of Exciton Luminescent ZnO Nanocrystals Using Continuous Supercritical Microfluidics**

*Yann Roig, Samuel Marre, Thierry Cardinal, and Cyril Aymonier**

ZnO has been extensively studied because of its applications in photovoltaics,[1] catalysis,[2] and optoelectronics.[3] Over the last two decades, the interest has been focused on ZnO high-efficiency UV photoluminescence (PL)[4] for the development of light-emitting diodes (LEDs) and lasers[5] or gas sensors.[6] Typical emission spectra of ZnO at room temperature show an emission band localized in the UV domain ($\lambda \approx 360$ to 380 nm, that is, 3.18 to 3.43 eV), which is attributed to the excitonic recombination, whereas a broad band centered at $\lambda = 500$–$600$ nm (2.07–2.48 eV) corresponds to crystal and surface defects.[7] Other bands located in the range of $400 < \lambda < 500$ nm are also reported when surfactants are used because of surface hole trapping effects.[8]

A large variety of ZnO micro- and nanostructures morphologies have been synthesized so far[9] using several processes including chemical or physical vapor deposition,[9a] pulsed laser deposition,[10] spray pyrolysis,[11] sol–gel[12] and liquid-phase processes,[9] hydrothermal[13] and supercritical fluids.[14] Most ZnO materials synthesized through liquid-phase methods show controlled sizes (from few nanometers to several hundreds of nanometers) and morphologies, taking advantages of the well-developed batch processes and the large amount of surfactant systems available.[15] However, the low operating temperatures lead to a certain amount of defects within the synthesized nanocrystals (NCs). These defects induce poor excitonic but strong defect visible photoluminescence, incompatible with several applications—such as UV-LEDs—requiring controlled UV emitters. Oppositely, intense excitonic luminescent ZnO materials are obtained mostly through high-temperature gas-phase synthetic methods.[16] However, these processes have a poor control over the size of the synthesized particles.[17] Consequently, supercritical fluids (SCFs) are potentially ideal solvents for such syntheses, providing means for solution-based processes in an environment that behaves like a gas.[18] The synthesis of ZnO nanostructures has been reported in SCFs, showing the feasibility of the process. The few examples reported so far were performed in supercritical (sc) water[14a,19] or sc methanol.[14b] However, the PL and surface properties were hardly investigated, still showing defect luminescence.[14a]

To improve the reproducibility of the process and to get better control over the ZnO NC properties, it is advantageous to take benefits of continuous synthetic methods based on microfluidics. These methods offer several advantages, which have already been applied to the synthesis of various nanostructures,[20] including ZnO microparticles.[21] The recent development of microreactors withstanding high-pressure/high-temperature conditions has opened opportunities for coupling microfluidic tools with supercritical fluids processes ("supercritical microfluidics"—SCμF) for synthesizing nanostructures.[22] This approach was successfully applied to obtain high-quality CdSe[22a,23] and InP[24] quantum dots with narrow particles size distributions (PSD).

Herein we develop an original microfluidic process to synthesize exciton luminescent ZnO NCs. The advanced optical properties of the as-synthesized ZnO nanostructures are obtained thanks to their nucleation and growth in supercritical fluids and to the separation of nucleation/growth and functionalization steps,[25] both being performed in a hydrodynamically controlled environment provided by microreactors.[20a,22b] Several operating parameters have been investigated: 1) the ligand (oleylamine—OL, trioctylphosphine—TOP and oleic acid—OA), 2) the ligand-to-zinc molar ratio ($R_L$), 3) the oxidant-to-zinc molar ratio ($R_{Ox}$), and 4) the fluid velocity ratio $R_H = V_{int}/V_{ext}$. In all cases, the correlation between NP characteristics and their photoluminescence properties is discussed.

The experiments were carried out in a coaxial flowing microsystem made of two fused silica capillaries (inner diameters: $\varnothing_1 = 100$ μm, $\varnothing_2 = 250$ μm, length = 1 m) as shown in Figure 1 A. Heating was provided by an oil bath ($T = 250$ °C), whereas the pressure was controlled with a back-pressure regulator downstream ($p = 25$ MPa). The precursor solution—$[Zn(acac)_2]\cdot H_2O$ ($10^{-2}$ M) in an ethanol solution containing $H_2O_2$ ($10^{-2}$–$10^{-1}$ M $H_2O_2$ from a 35 wt% $H_2O_2$/water solution)—is injected in the inner silica capillary. A second solution containing ligands ($6.10^{-2}$–$4.5.10^{-1}$ M—TOP, OL or OA) in ethanol is injected externally, the overall residence time being fixed at 10 s. The coaxial injection ensures a 3D positioning of the precursor flow at the center of the main tubing, as exemplified with a dye flow used for visualization (Figure 1 B).

The addition of $H_2O_2$ accelerates the hydrolysis of $[Zn(acac)_2]\cdot H_2O$, confining the nucleation and growth of ZnO NCs in the inner flow, followed by surfactant capping achieved downstream upon mixing/diffusion of the two coaxial flows. The combined use of coaxial injection and $H_2O_2$ addition is necessary to prevent clogging because of

[*] Y. Roig, Dr. S. Marre, Dr. T. Cardinal, Dr. C. Aymonier
CNRS, Université de Bordeaux, ICMCB
87 avenue du Dr. A. Schweitzer, 33607 Pessac (France)
E-mail: aymonier@icmcb-bordeaux.cnrs.fr

[**] The author acknowledges the support of the French Agence Nationale de la Recherche (ANR), under grants SCμF (grant number ANR-09-BLAN-0105-01) "Supercritical Microfluidics" and AMOS (grant number ANR-10-BLAN-0820) "Advanced Materials for Optical Sensors" and of the GIS "Advanced Materials in Aquitaine".

Supporting information for this article is available on the WWW under http://dx.doi.org/10.1002/anie.201106201.

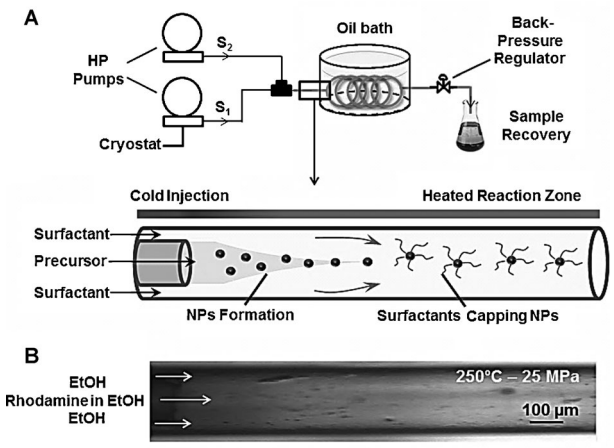


***Figure 1.*** A) Experimental supercritical microfluidics setup with enlargement of the coflowing injection method developed (HP = high pressure, $S_1$ = precursor solution, and $S_2$ = ligand solutions. The latter is exemplified with an ethanol/rhodamine dye in ethanol coflow at 250 °C and 25 MPa (B).

either NPs deposition or decomposition of unreacted Zn precursor onto the walls. This method addresses the clogging limitations encountered in most microfluidic application for handling solids.[26]

A typical TEM micrograph of ZnO-TOP NCs is shown in Figure 2 A. Small ($3.7 \pm 0.5$ nm) spherical nanocrystals are obtained. The electron diffraction pattern corresponds to pure wurtzite-type ZnO, which was confirmed by Raman spectroscopy (see the Supporting Information). The associated photoluminescence (PL) spectrum exhibits only one narrow peak ($E = 3.30$ eV) attributed to excitonic recombination with sub-microsecond lifetime (Figure 2 B), whereas no broad emission related to defect states is observed below the band gap.

This is to be compared with 1) size and shape-controlled ZnO NCs synthesized through conventional low-temperature liquid-phase methods,[27] for which a low-intensity excitonic peak is generally observed combined with large defect luminescence centered at 2.20 eV ($\lambda = 600$ nm) and 2) large crystalline ZnO nanostructures with exciton PL obtained through high-temperature gas-phase synthetic approaches[28] (Figure 2 B). Note that other authors reported spray pyrolysis synthesis of agglomerated ZnO NPs without conducting PL studies.[17b] The results obtained herein confirm the advantage of SCμF for synthesizing well-controlled crystalline ZnO nanostructures taking advantage of solution-based chemistry for a better control of the size and shape of the NPs and of high-temperature gas-phase approaches providing good crystallinity and stoichiometry, and therefore exciton PL.

The influence of the functional group of the ligand was investigated by switching from phosphorous to amine and carboxylic acid using TOP, OL, and OA, respectively. In all cases, electron diffraction and Raman spectroscopy confirmed the presence of pure wurtzite-type ZnO NCs (see the Supporting Information). Figure 3 A, B shows TEM pictures of the ZnO–OL and ZnO–OA NPs. Negligible size changes are observed for the ZnO NPs ($3.5 \pm 0.4$ nm and $3.9 \pm 0.7$ nm

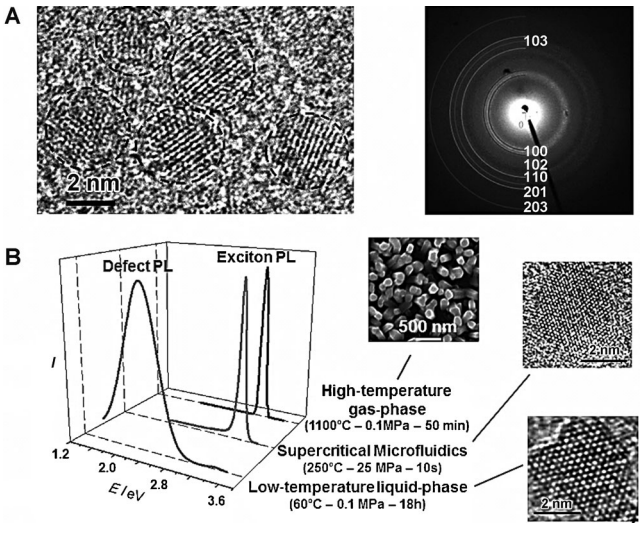


***Figure 2.*** A) HRTEM and electron diffraction snapshot of ZnO/TOP NCs obtained for $R_{Ox} = 2/1$, $R_L = 6/1$, and $R_H = 0.6$. B) Comparison of the PL of ZnO nanostructures obtained through various methods: high-temperature gas-phase, low-temperature liquid-phase, and supercritical microfluidic methods for $\lambda_{excitation} = 320$ nm.

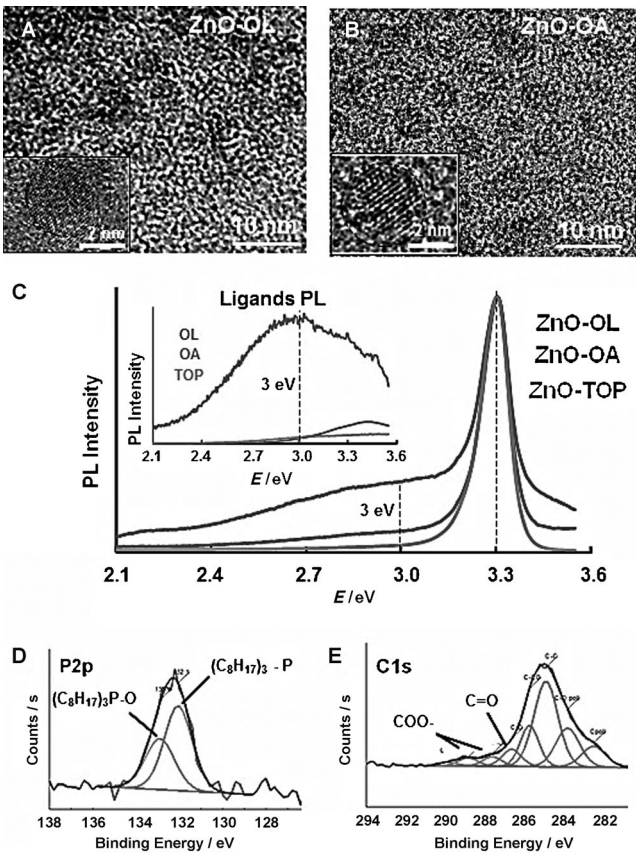


***Figure 3.*** HRTEM snapshots of A) ZnO–OL and B) ZnO–OA NPs both obtained for $R_L = 6/1$, $R_{Ox} = 2/1$, and $R_H = 0.6$. C) Comparison of the PL properties of ZnO–ligands and pure ligands (inset). D,E) P2p and C1s XPS spectra for ZnO–TOP and ZnO–OA samples, respectively.

  

for ZnO–OL and ZnO–OA, respectively). All the PL spectra of ZnO–ligand NCs show a single excitonic peak located at 3.30 eV ($\lambda = 376$ nm; Figure 3C), while no defect band is detected. Note, however, that for ZnO–OL a shoulder is observed at around 3 eV, which can be attributed to the OL PL. This hypothesis was confirmed by performing PL analysis on pure ligands (OL, OA, and TOP—see inset in Figure 3C). OL alone shows a wide strong PL centered at around 3 eV, which could be mainly responsible for the shoulder observed in the photoluminescence of the ZnO–OL QDs. In comparison, OA and TOP have much weaker PL emissions, typically one order a magnitude lower, with little influence on the final photoluminescence of the NPs.

X-ray photoelectron spectroscopy (XPS) was used to get further information on the surface chemistry of ZnO NCs for the experiments performed with TOP or OA as ligands. XPS analysis of ZnO–TOP NPs (Figure 3D) confirms the presence of phosphorous. The spectra can be fitted by two functions, of which one is assigned to phosphorous atoms in a low oxygen environment ($E = 133$ eV), suggesting possible bonds between the phosphorous atom of TOP and the ZnO NP surface (ZnO–P). For ZnO–OA (Figure 3E), the C1s XPS spectra show the presence of several contributions among which are contributions from C=O and $COO^-$ bonds, corresponding to oleic acid ligands. However, nitrogen is not detected for ZnO–OL, because we reach the detection limit of the XPS technique for this atom. All the above-mentioned peaks disappeared upon $Ar^+$ ion etching of the surface, confirming the surface location of the ligands.

The influence of $R_{Ox}$ on the ZnO–OL NCs is reported in Figure 4A. Experiments for $R_{Ox} \leq 1$ are not reported because they lead to clogging after few minutes, supporting the interest of adding an oxidant to form ZnO in the "bulk" fluid and not on the reactor wall. Clogging is avoided for $R_{Ox} \geq 2$, for which value we can assume—under our working conditions—that enough $H_2O_2$ is injected to induce the hydrolysis of the zinc precursor.[29] For all other experiments ($R_{Ox} \geq 2$), the single excitonic PL peak is observed in each case without being shifted. Additionally, increasing $R_{Ox}$ results in the appearance and further increase of emission bands located at 2.96, 2.85, and 2.67 eV, respectively. Although it is still unclear to which bonds these bands can be related, assumptions can be made concerning the formation of organic compounds from the reaction between OL and $H_2O_2$ at high temperatures. However, $R_{Ox}$ has neither influence on the size of the ZnO NPs, nor on the structure (wurtzite-type), therefore, $R_{Ox} = 2/1$ was the optimum value retained in this study.

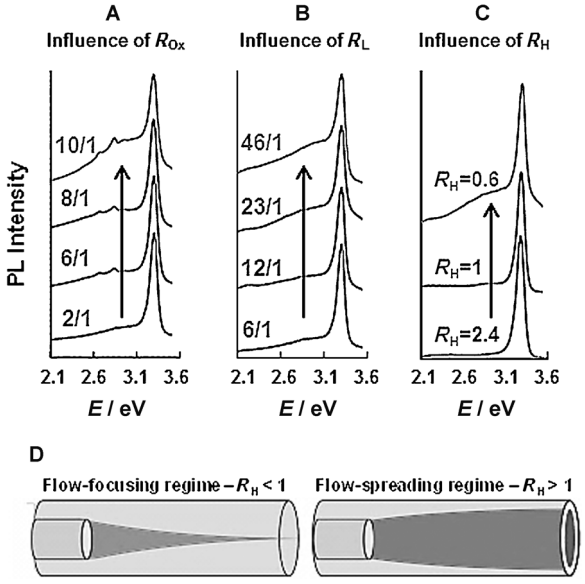


***Figure 4.*** Evolution of photoluminescence spectra ($\lambda_{exc} = 320$ nm) with A) the oxidant-to-zinc molar ratio ($R_{Ox}$), B) the ligand-to-zinc molar ratio ($R_L$), and C) the fluid velocity ratio $R_H = V_{int}/V_{ext}$. D) The two considered flow regimes: flow-focusing ($R_H < 1$) and flow-spreading ($R_H > 1$) regimes.

The fast screening capability of the microfluidic approach was later used to study the influence of the ligand-to-zinc molar ratio ($R_L$). $R_L$ was varied from 6/1 to 46/1 choosing OL as reference ligand, because it exhibits high PL, while all other parameters are kept constant (i.e. $R_{Ox} = 2/1$, $R_H = 0.6$). From TEM observations, no changes are noticed concerning the size of the ZnO NPs. As expected, the respective PL spectra (Figure 4B) show an increase in the PL shoulder because of OL ($E \approx 3$ eV, see black arrow) when $R_L$ increases. This study shows that control of the concentration of the added ligands without changing the characteristics of the as-synthesized NCs is possible using this approach, which separates the nucleation/growth and functionalization steps. From the obtained results, a low (6/1) ligand-to-zinc molar ratio is enough to obtain well-stabilized and dispersible ZnO NCs.

Hydrodynamics gains increasing importance in such microscale coflowing synthesis processes. The influence of the ratio of the internal to external flow velocities over the NC size and PL properties was therefore investigated. We tuned the average velocity of internal to external flow from a flow-focusing ($R_H < 1$) to a flow-spreading regime ($R_H > 1$; Figure 4D), while all other parameters were kept constant (i.e. $R_{Ox} = 2/1$, $R_L = 6/1$, ligand: OL). For $R_H = 2.4$, the average size of the particles remains the same ($\approx 4$ nm). However, increasing $R_H$ results in an agglomeration of the ZnO NCs, which can be attributed to the longer time required for the ligands to access the ZnO NC surface in the flow-spreading regime. PL spectra of the ZnO–OL NPs for $R_H = 0.6$, 1, and 2.4 are shown in Figure 4C. Few differences can be noticed between $R_H = 1$ and $R_H = 2.4$, however, the intensity of the OL contribution to the PL spectra (shoulder at $E \approx 3$ eV) is much more pronounced in the flow-focusing regime ($R_H = 0.6$), for which more ligands can actually access the NC surface, prior to agglomeration.

To conclude, we have demonstrated a new way to obtain UV emitting ZnO NCs with pure excitonic photoluminescence using SCμF. The conventional clogging limitation of the microchannels was overcome by hydrodynamic control over the environment provided by the microreactors and by enhanced hydrolysis of the zinc precursor with $H_2O_2$. The influence of several operating parameters was carefully studied showing the separation of nucleation/growth from functionalization steps. This method therefore allows for easily interchanging capping ligands without influencing the

  

ZnO NCs size or structure (wurtzite structure in each case). The ZnO NCs PL spectra display the same excitonic peak, sometimes coupled to the PL contribution of the ligands, in particular when amines are considered. We believe these UV emitting ZnO NCs are useful for applications as UV LEDs or gas sensors, which are the subject of our ongoing work.

## Experimental Section

Preparation of precursor and surfactant solution: The precursor solution ($S_1$) was prepared ($10^{-2}$ M) of zinc acetylacetonate monohydrate ($[Zn(acac)_2]\cdot H_2O$) purchased from Sigma–Aldrich and different ratios ($H_2O_2$:Zn, namely $R_{Ox}$) of $H_2O_2$ at 35 wt% in water purchased from Sigma–Aldrich, all diluted in absolute ethanol. The surfactant solution ($S_2$) was prepared considering the dilution in the capillaries of the precursor solution. Oleylamine, trioctyphosphine, and oleic acid were purchased from Sigma–Aldrich and diluted in ethanol.

Purification of the nanoparticles: The solution of the ZnO NPs was centrifuged at 9000 rpm during 30 min and redispersed in pentane or dried in air.

Characterization techniques: TEM and high resolution (HR) TEM were performed using a HITACHI H7650 and a JEOL 2200 FS, respectively, equipped with a field emission gun, operating at 200 kV and with a point resolution of 0.23 nm. X-ray photoelectron spectra were taken with an ESCALAB 220iXL from VG, a RX source TWIN Mg (1253.6 eV), and surveys of 150 eV. The analyzed area is a circle with a diameter of 150 μm. High-resolution spectra were obtained with an energy $E_p$ of 40 eV. The samples were obtained by pressing a small amount of powder on indium foils. Spectra were exploited with the AVANTAGE software from Thermo Fisher Scientific. Photoluminescence spectra were obtained using a Jobin Yvon SPEX spectrofluorometer (Fluorolog 212) equipped with a double monochromator and a xenon lamp. ZnO powder was set between two quartz slides and exposed in the device $\lambda_{excitation} = 320$ nm. Raman spectra were obtained using a Thermo scientific DXR micro-Raman spectrometer at an excitation wavelength of 532 nm and a laser power of 10 mW.

Received: September 1, 2011
Published online: October 21, 2011

**Keywords:** microfluidics · nanocrystals · photoluminescence · supercritical fluids

[1] Z. S. Wang, C. H. Huang, Y. Y. Huang, Y. J. Hou, P. H. Xie, B. W. Zhang, H. M. Cheng, *Chem. Mater.* **2001**, *13*, 678 – 682.
[2] a) M. Kurtz, J. Strunk, O. Hinrichsen, M. Muhler, K. Fink, B. Meyer, C. Woell, *Angew. Chem.* **2005**, *117*, 2850 – 2854; *Angew. Chem. Int. Ed.* **2005**, *44*, 2790 – 2794; b) J. A. Rodriguez, P. Liu, J. Hrbek, J. Evans, M. Perez, *Angew. Chem.* **2007**, *119*, 1351 – 1354; *Angew. Chem. Int. Ed.* **2007**, *46*, 1329 – 1332.
[3] A. Tsukazaki, A. Ohtomo, T. Onuma, M. Ohtani, T. Makino, M. Sumiya, K. Ohtani, S. F. Chichibu, S. Fuke, Y. Segawa, H. Ohno, H. Koinuma, M. Kawasaki, *Nat. Mater.* **2005**, *4*, 42 – 46.
[4] T. Andelman, Y. Y. Gong, M. Polking, M. Yin, I. Kuskovsky, G. Neumark, S. O'Brien, *J. Phys. Chem. B* **2005**, *109*, 14314 – 14318.
[5] D. M. Bagnall, Y. F. Chen, Z. Zhu, T. Yao, S. Koyama, M. Y. Shen, T. Goto, *Appl. Phys. Lett.* **1997**, *70*, 2230 – 2232.
[6] C. Baratto, S. Todros, G. Faglia, E. Comini, G. Sberveglieri, S. Lettieri, L. Santamaria, P. Maddalena, *Sens. Actuators B* **2009**, *140*, 461 – 466.
[7] a) A. B. Djurišić, W. C. H. Choy, V. A. L. Roy, Y. H. Leung, C. Y. Kwong, K. W. Cheah, T. K. G. Rao, W. K. Chan, H. T. Lui, C. Surya, *Adv. Funct. Mater.* **2004**, *14*, 856 – 864; b) A. van Dijken, E. A. Meulenkamp, D. Vanmaekelbergh, A. Meijerink, *J. Lumin.* **2000**, *90*, 123 – 128.
[8] M. L. Kahn, T. Cardinal, B. Bousquet, M. Monge, V. Jubera, B. Chaudret, *ChemPhysChem* **2006**, *7*, 2392 – 2397.
[9] a) Z. L. Wang, *Mater. Sci. Eng. R* **2009**, *64*, 33 – 71; b) M. Monge, M. L. Kahn, A. Maisonnat, B. Chaudret, *Angew. Chem.* **2003**, *115*, 5479 – 5482; *Angew. Chem. Int. Ed.* **2003**, *42*, 5321 – 5324.
[10] C. Y. Lo, J. S. Hwang, X. M. Liu, Y. Y. Zhang, D. C. Chen, C. C. Wu, T. Y. Lin, S. Chattopadhyay, *J. Cryst. Growth* **2010**, *312*, 3564 – 3568.
[11] T. Q. Liu, O. Sakurai, N. Mizutani, M. Kato, *J. Mater. Sci.* **1986**, *21*, 3698 – 3702.
[12] D. Mondelaers, G. Vanhoyland, H. Van den Rul, J. D'Haen, M. K. Van Bael, J. Mullens, L. C. Van Poucke, *Mater. Res. Bull.* **2002**, *37*, 901 – 914.
[13] T. Mousavand, S. Ohara, T. Naka, M. Umetsu, S. Takami, T. Adschiri, *J. Mater. Res.* **2010**, *25*, 219 – 223.
[14] a) S. Ohara, T. Mousavand, T. Sasaki, M. Umetsu, T. Naka, T. Adschiri, *J. Mater. Sci.* **2008**, *43*, 2393 – 2396; b) B. Veriansyah, J. D. Kim, B. K. Min, Y. H. Shin, Y. W. Lee, J. Kim, *J. Supercrit. Fluids* **2010**, *52*, 76 – 83.
[15] H. Usui, *Mater. Lett.* **2009**, *63*, 1489 – 1492.
[16] E. Karber, T. Raadik, T. Dedova, J. Krustok, A. Mere, V. Mikli, M. Krunks, *Nanoscale Res. Lett.* **2011**, *6*, 359.
[17] a) I. M. Joni, A. Purwanto, F. Iskandar, M. Hazata, K. Okuyama, *Chem. Eng. J.* **2009**, *155*, 433 – 441; b) S. Turner, S. M. F. Tavernier, G. Huyberechts, E. Biermans, S. Bals, K. J. Batenburg, G. Van Tendeloo, *J. Nanopart. Res.* **2010**, *12*, 615 – 622.
[18] a) F. Cansell, C. Aymonier, *J. Supercrit. Fluids* **2009**, *47*, 508 – 516; b) S. Marre, F. Cansell, C. Aymonier, *Nanotechnology* **2006**, *17*, 4594 – 4599.
[19] a) T. Adschiri, Y. W. Lee, M. Goto, S. Takami, *Green Chem.* **2011**, *13*, 1380 – 1390; b) M. Søndergaard, E. D. Bøjesen, M. Christensen, B. Iversen, *Cryst. Growth Des.* **2011**, *11*, 4027 – 4033.
[20] a) S. Marre, K. F. Jensen, *Chem. Soc. Rev.* **2010**, *39*, 1183 – 1202; b) A. M. Nightingale, J. C. de Mello, *J. Mater. Chem.* **2010**, *20*, 8454 – 8463; c) J. Il Park, A. Saffari, S. Kumar, A. Gunther, E. Kumacheva, *Annu. Rev. Mater. Res.* **2010**, *40*, 415 – 443; d) A. Abou-Hassan, O. Sandre, V. Cabuil, *Angew. Chem.* **2010**, *122*, 6408 – 6428; *Angew. Chem. Int. Ed.* **2010**, *49*, 6268 – 6286.
[21] S. Li, G. A. Gross, P. M. Gunther, J. M. Kohler, *Chem. Eng. J.* **2011**, *167*, 681 – 687.
[22] a) S. Marre, J. Baek, J. Park, M. G. Bawendi, K. F. Jensen, *JALA* **2009**, *14*, 367 – 373; b) S. Marre, A. Adamo, S. Basak, C. Aymonier, K. F. Jensen, *Ind. Eng. Chem. Res.* **2010**, *49*, 11310 – 11320.
[23] S. Marre, J. Park, J. Rempel, J. Guan, M. G. Bawendi, K. F. Jensen, *Adv. Mater.* **2008**, *20*, 4830 – 4834.
[24] J. Baek, P. M. Allen, M. G. Bawendi, K. F. Jensen, *Angew. Chem.* **2011**, *123*, 653 – 656; *Angew. Chem. Int. Ed.* **2011**, *50*, 627 – 630.
[25] S. Moisan, J. D. Marty, F. Cansell, C. Aymonier, *Chem. Commun.* **2008**, 1428 – 1430.
[26] R. L. Hartman, J. R. Naber, N. Zaborenko, S. L. Buchwald, K. F. Jensen, *Org. Process Res. Dev.* **2010**, *14*, 1347 – 1357.
[27] W. M. Huang, P. Jiang, C. Y. Wei, D. K. Zhuang, J. L. Shi, *J. Mater. Res.* **2008**, *23*, 1946 – 1952.
[28] M. Krunks, T. Dedova, E. Karber, V. Mikli, I. O. Acik, M. Grossberg, A. Mere, *Physica B* **2009**, *404*, 4422 – 4425; Y. Qiu, L. Z. Hu, D. Q. Yu, H. Q. Zhang, J. C. Sun, B. Wang, J. X. Ma, L. N. Wang, K. T. Sun, Z. W. Zhao, *Micro Nano Lett.* **2010**, *5*, 251 – 253.
[29] E. Croiset, S. F. Rice, R. G. Hanush, *AIChE J.* **1997**, *43*, 2343 – 2352.

  